Research Article | Vol. 32, No. 24 / 18 Nov 2024 / Optics Express 42368
Optics EXPRESS

Generation of pseudo-nondiffracting symmetrical Layer beams using cylindrical lenses

MARTIN DUŠEK,[1,2,*] SEBASTIAN FIGURA,[1,3] JEAN-CHRISTOPHE GAYDE,[1] AND MIROSLAV ŠULC[2,4]

[1]The European Organization for Nuclear Research (CERN), Geneva, Switzerland
[2]Technical University of Liberec (TUL), Liberec, Czech Republic
[3]Cracow University of Technology (CUT), Cracow, Poland
[4]Institute of Plasma Physics of the Czech Academy of Sciences (IPP CAS), Prague, Czech Republic
[*]martin.dusek@cern.ch

Abstract: The pseudo-nondiffracting behavior of optical caustic beams makes them potentially useful in precise component alignment at CERN. This paper introduces an innovative method for generating one and two-dimensional symmetrical Airy-like beams, known as Layer beams, utilizing a specific configuration of plano-convex cylindrical lenses. Simulations and experimental results have validated this method, demonstrating its potential for scalable and cost-effective beam production with tunable properties, making it practical for a wide range of scientific applications.

1. Introduction

Optical caustic is a well-known phenomenon present in everyday life every time light is reflected or refracted by curved surfaces [1,2]. Similarly, optical caustic beams (OCB) [3] are characterized by wavefronts, hence ray envelopes, which cause the rays to overlap in a specific way creating caustic beam trajectories, due to the superposition of different wavefront parts. These beams exhibit interesting properties, including pseudo-nondiffracting behavior and the capacity for regeneration beyond obstacles.

The behavior of OCBs can be explained by catastrophe theory, where the ray envelopes are structurally stable singularities. It allows for the so-called fold and cusp caustics. An example of fold-type caustics is an Airy beam [4], having the ray envelope characterized by a cubic power. After their subsequent empirical validation [5], extensive research has been dedicated to elucidating the properties and exploring the diverse applications of such beams. These include light-sheet microscopy [6], particle manipulation [7], plasma channel generation [8], and other areas [9].

Cusp-like beams are characterized by even symmetry of the ray envelope. Examples of these beams are the symmetric Airy beams [10,11], the Pearcey-Gaussian beams [12], and the symmetric Swallowtail beams [13]. They can be imagined as two Airy-like beams with opposing acceleration directions.

The state-of-the-art approach to generating the aforementioned beams involves using a Gaussian beam incident on a spatial light modulator encoded with an angular phase of the desired beam, coupled with a lens performing a spatial Fourier transformation, or by encoding a computer-generated hologram on the spatial light modulator [5,10,11,13]. Alternatively, diverse methodologies utilizing specialized off-the-shelf components were shown [14–23]. Although previous studies have reported the potential for straightforward Airy-like beam generation using

#537554 https://doi.org/10.1364/OE.537554
Journal © 2024 Received 26 Jul 2024; revised 20 Sep 2024; accepted 22 Sep 2024; published 5 Nov 2024

Optics EXPRESS

standard cylindrical lenses [24–27], the generation of cusp caustic beams through a similar approach remains unexplored, as far as our knowledge extends.

At CERN, pseudo-nondiffracting beams are currently under extensive investigation regarding their utility in aligning accelerator components [28–31] and particle acceleration applications [32]. OCBs, with their distinctive properties, hold promise to be used as a multi-point reference for the alignment of accelerator parts at CERN similar to the wire positioning and hydrostatic leveling system [33]. Our previous research focused on the use of the so-called Structured laser beam [28,34] for this purpose, which can generate a reference line. Layer beams offer an advantage in multi-point alignment as they create a reference plane, which can ease the detection of multiple points at one moment in time over a long distance. Given the vast nature of the accelerator complex, a simple, scalable, and cost-effective solution for generating such beams is highly desirable. This paper presents a novel method for generating so-called one-dimensional and two-dimensional beams, using various configurations of plano-convex cylindrical lenses. These beams, referred to as Layer beams, address the specified requirements.

2. Methodology

The generation of a Layer beam involves a series of cylindrical lenses, as depicted in Fig. 1. The initial lens in the sequence, referred to as the phase lens, is illuminated by a Gaussian beam. This lens functions analogously to a spatial light modulator, acting as an angular phase modulator in the spectral domain. Consequently, the light in the Fourier plane located at the focal length F_{PL} of the projection lens, and in the distance L_{Ph} from the phase lens, undergoes a spatial Fourier transformation by the projection lens [35].

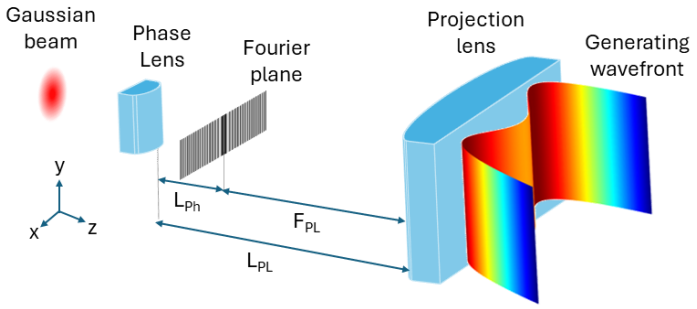

Fig. 1. One-dimensional Layer beam generator.

The generation principle can also be explained by analyzing the phase delay that is introduced by the generator, which results in the creation of a so-called generating wavefront directly behind the projection lens. This enables the intersection of rays, resulting in the creation of a beam with desired properties through the superposition of different parts of the generating wavefront.

The Layer beams can be characterized either through the angular spectrum behind the phase lens or by the generating wavefront directly behind the projection lens. In the context of this paper, the generating wavefront approach is preferred in most of the explanations due to the generation principle using cylindrical lenses, as it can be measured using a wavefront sensor.

The generating wavefront dictates the caustic structure of the beam. Its shape is influenced by the distance L_{PL} between the lenses and their parameters, such as focal length or refractive index. Note that the distance L_{PL} also determines which phase plane undergoes the spatial Fourier transformation by the projection lens. The line profile of the generating wavefront can be

Optics EXPRESS

described using the equation:

$$W(x) = K_1 x^2 + \sum_{m=1}^{\infty} K_{m+1} x^{2(m+1)} \tag{1}$$

Equation (1) is directly related to optical aberrations induced by the lenses and by their position, specifically, the term with the squared power relates to defocus, and higher-order even terms correspond to various orders of spherical aberration. A change of the distance L_{PL} influences mainly the amount of the defocus in the system, which causes the generating wavefront to change shape, as will become evident in the following chapters.

Equation (1) describes the line profile of the generating wavefront of Layer beams. The line profile of the wavefront remains consistent when analyzed along the y-axis, as illustrated in Fig. 1. Consequently, describing the beam using the line profile alone is sufficient. This results in the formation of parallel lines in the transversal intensity distribution.

An additional cylindrical lens, rotated by 90 degrees around the optical axis, can be placed in front of the phase lens, as shown in Fig. 2(a). This lens is referred to as the dimension lens. This yields one-dimensional beams with the same profile of the transversal intensity distribution along the x-axis as if the dimension lens was not used, but with significantly elongated lines along the y-axis, as illustrated in Fig. 2(b). The length of these lines can be adjusted by varying the focal length and position of the dimension lens along the z-axis as it alters the divergence of the beam along the y-axis. This configuration can be beneficial in long-distance multi-point alignment applications as the size of the reference plane generated by the beam increases.

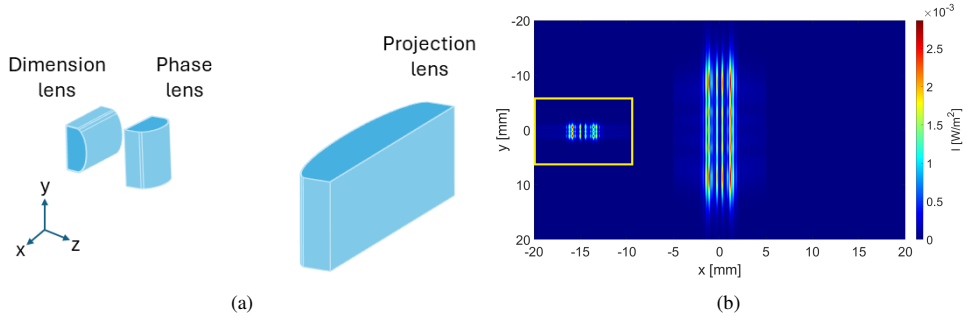

Fig. 2. (a) One-dimensional Layer beam generator with a dimension lens. (b) Simulated one-dimensional Layer beam prolonged in the y-axis generated using a generator with the dimension lens. A one-dimensional Layer beam is generated using the generator without the dimension lens for comparison in the yellow rectangle.

The equation can be extended to two dimensions by superposing two one-dimensional beams rotated by 90 degrees around the optical axis, generating two-dimensional Layer beams. Such beams can be created using a generator consisting of two phase lenses and two projection lenses, each additional lens rotated by 90 degrees around the optical axis, as illustrated in Fig. 3.

Extending the equations to cylindrical coordinates yields a so-called Structured laser beam [28,34], which can be generated using lenses with rotational symmetry. This beam has an intense central core surrounded by rings, which resembles the intensity distribution of a Bessel beam [36]. In our previous works, the generation method using a high refractive index ball lens, as the phase lens, together with a plano-convex lens, as the projection lens, was demonstrated.

All of the caustic beams described above can also be generated using a reflective or transmissive optical element, which would induce a phase delay similar to that of a generating wavefront. This could be achieved with a glass plate [16] or with a mirror [18]. However, the presented approach

Optics EXPRESS

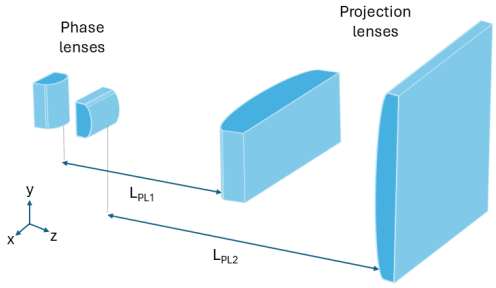

Fig. 3. Generator of two-dimensional Layer beams consisting of two phase and two projection lenses.

using a set of lenses allows for simple tunability of beam parameters by merely changing the L_{PL} distance.

3. Results

3.1. Simulations

To analyze the generator and beam properties, numerical simulations were performed using the commercially available software VirtualLab Fusion, which combines ray tracing and electromagnetic field propagation calculations. The simulated generator consisted of a plano-convex cylindrical phase lens with a focal length of 5.79 mm and another plano-convex cylindrical projection lens with a focal length of 20 mm. The lens material was N-BK7 glass. A Gaussian beam with a wavelength of 532 nm was used as a source and entered the system with a planar wavefront.

The dependence of the coefficients K_1 and K_2 of Eq. (1) on the distance L_{PL} can be seen in Fig. 4. Only the second and fourth power coefficients in Eq. (1) were used to model the wavefront line profile, as it yielded a sufficiently precise approximation. The line profile of the generating wavefront together with the longitudinal intensity distribution for different distances L_{PL} can be seen in Fig. 5 together with transversal intensity profiles at 0.4, 0.8, 1.2, and 1.6 m away from the generator in Fig. 6.

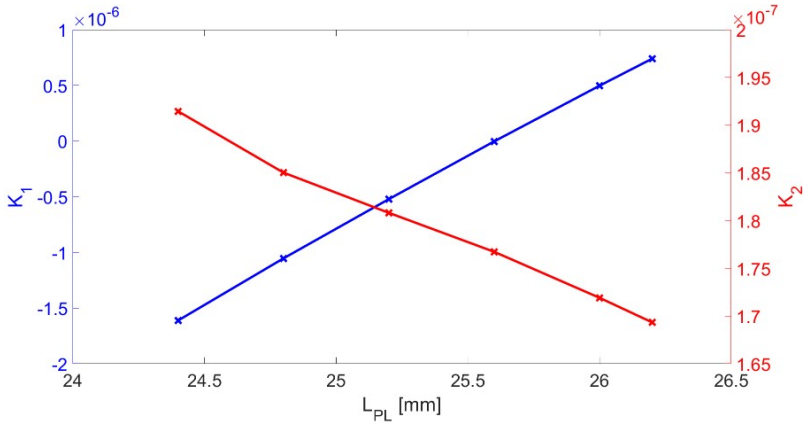

Fig. 4. Values of coefficients K_1, K_2 of Eq. (1) with respect to the L_{PL} distance.

Optics EXPRESS

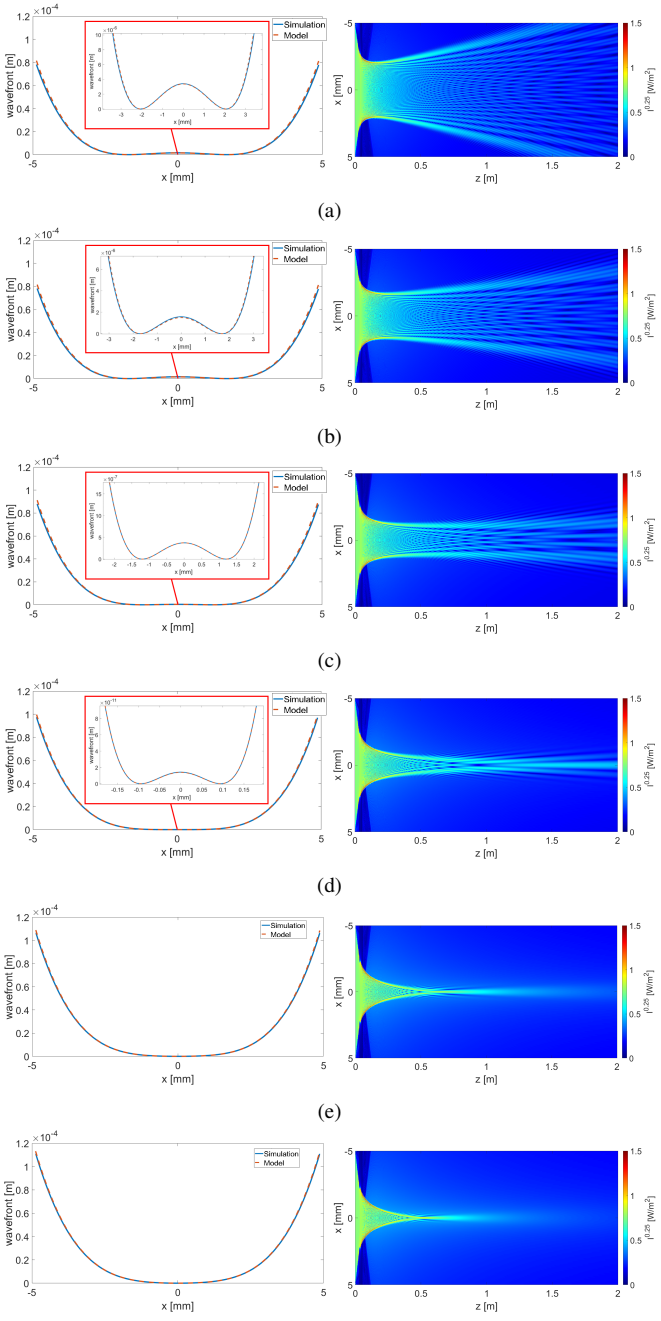

Fig. 5. A generating wavefront with the modeled wavefront according to Eq. (1) (left) and longitudinal intensity profile (right) for the L_{PL} distance of (a) 24.4 mm, (b) 24.8 mm, (c) 25.2 mm, (d) 25.6 mm, (e) 26.0 mm, and (f) 26.2 mm. The intensity was enhanced for better visibility.

Optics EXPRESS

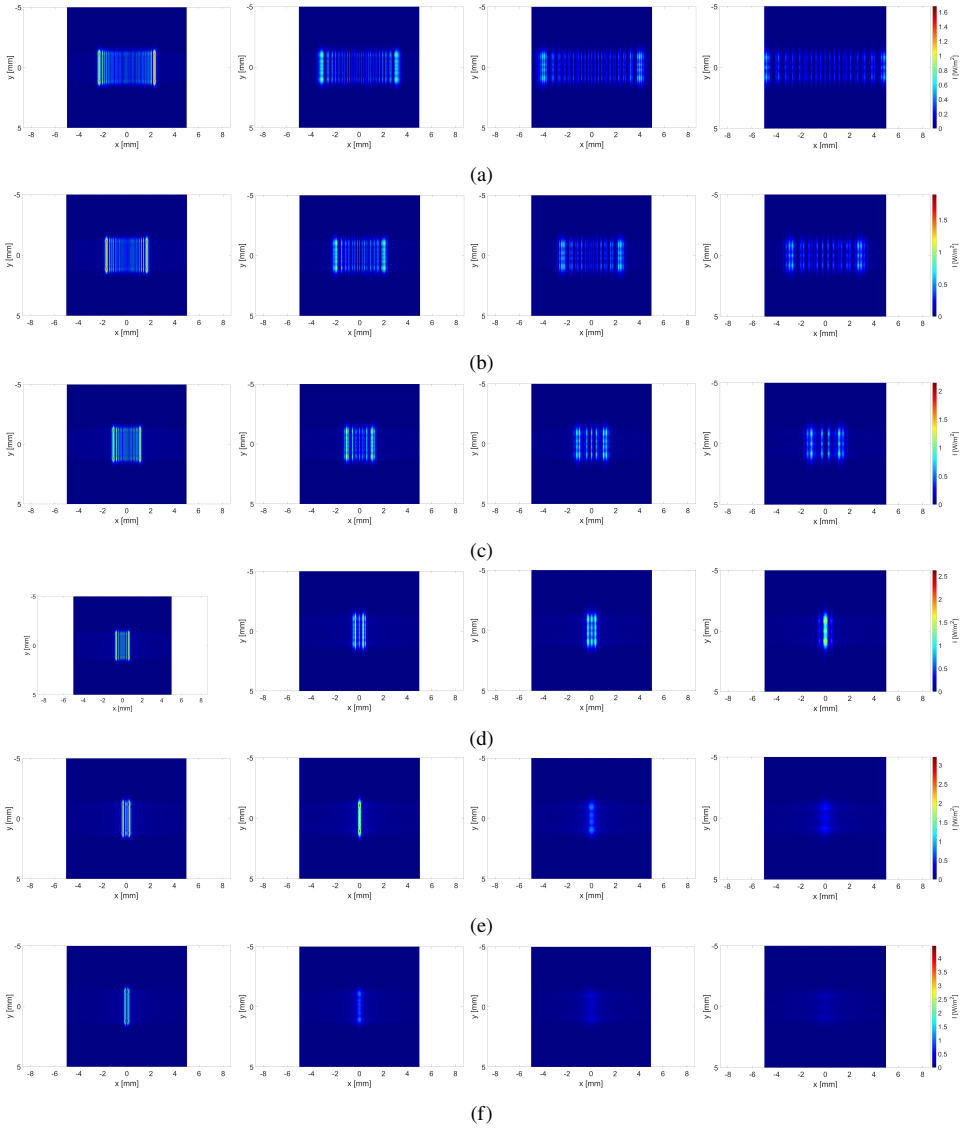

Fig. 6. Transversal intensity profile of one-dimensional Layer beams at the distance of 0.4 m, 0.8 m, 1.2 m and 1.6 m from the generator for the distance L_{PL} equal to (a) 24.4 mm, (b) 24.8 mm, (c) 25.2 mm, (d) 25.6 mm, (e) 26.0 mm, and (f) 26.2 mm.

Optics EXPRESS

The wavefront for the L_{PL} distances equal to 26.2 and 26.0 mm is converging. The coefficients K_1 and K_2 in Eq. (1) are both positive, hence the generating wavefront has no local extremes, and the beams propagate over a limited distance. As the L_{PL} distance increases, the beam travels over a shorter distance due to the higher slope of the wavefront, which is caused mainly by the change of the defocus coefficient K_1. This can be seen in Figs. 5(e), 5(f), 6(e), and 6(f).

Once the distance L_{PL} gets shorter than 25.6 mm the generating wavefront takes on a "sombrero" shape with two local minima and local maximum at the optical axis. The local minima get farther apart as the L_{PL} distance shortens and the absolute phase difference between the local minimum and maximum increases. This is caused by the fact that the defocus coefficient K_1 becomes negative and decreases as the distance L_{PL} shortens, while the spherical aberration coefficient K_2 remains positive (Fig. 4). These beams propagate to infinity (Figs. 5(a), 5(b), 5(c), 5(d), 6(a), 6(b), 6(c) , and 6(d)).

A more detailed analysis of the generating wavefront shape provides further insight into the propagation properties of the Layer beam. It is possible to trace the rays starting from the wavefront as according to the Eikonal equation, the rays are locally perpendicular to it [37]. Different parts of the generating wavefront are illustrated in Fig. 7. Regions of the Layer beam along the propagation distance are shown in Fig. 8. The intensity distribution of the beam undergoes rapid changes in the near zone, where a significant number of rays from the outer parts of the wavefront intersect with rays from other parts of the wavefront. In this area, the beam exhibits pseudo-nondiffracting properties and can regenerate behind reasonably sized obstacles, provided the obstacle does not block the majority of the beam. The outer part of the beam exhibits strong curvature. Conversely, in the diverging zone, the transversal intensity distribution remains unchanged, only diverging as rays from regions with low wavefront gradients intersect. The outer part of the beam straightens in this zone.

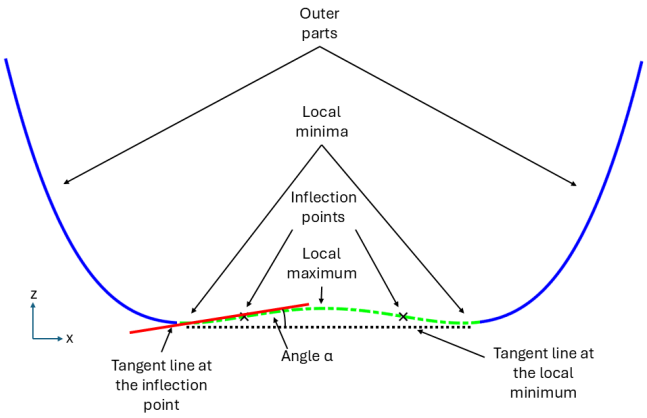

Fig. 7. Description of the generating wavefront regions.

Figures 9(a), 9(b), and 9(c) show rays originating from the generating wavefront, along with the corresponding longitudinal profiles, for propagation distances L_{PL} of 24.4, 25.6, and 26.0 mm, respectively. As mentioned in the previous text, the Layer beam is composed of two Airy-like beams with opposing acceleration directions. As the outer parts of the Airy-like beams straighten, rays originating from inflection points begin to align with the outer parts of the beam. These rays are plotted in red.

Figure 5 illustrates that the absolute phase difference between local minima and maxima increases by several orders of magnitude as the distance L_{PL} decreases. Additionally, local minima get farther apart, although only by approximately one order of magnitude. This leads to a steeper wavefront slope at the inflection points, resulting in an increase of the angle α (Fig. 7).

Optics EXPRESS

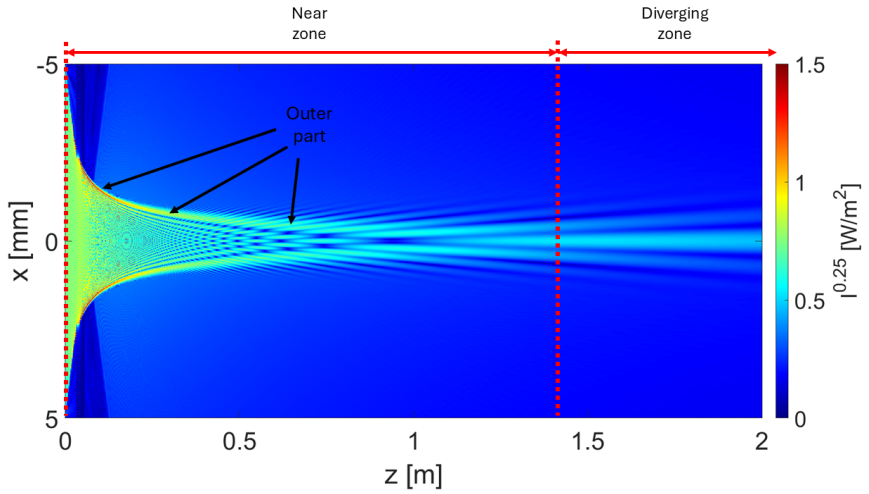

Fig. 8. Different regions along the Layer beam propagation distance.

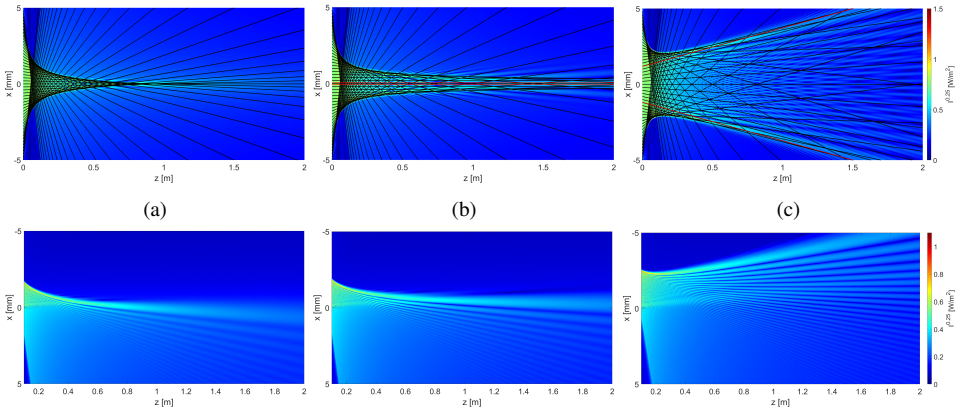

Fig. 9. Longitudinal profiles of one-dimensional Layer beams with rays plotted in black along with rays originating from inflection points in red for the distances L_{PL} equal to (a) 26.0 mm, (b) 25.6 mm, and (c) 24.4 mm. The longitudinal profiles on one of the Airy-like beams that form the Layer beam for the distances L_{PL} equal to (d) 26.0 mm, (e) 25.6 mm, and (f) 24.4 mm. The intensity was enhanced and profiles of Airy-like beams slightly zoomed in for better visibility.

Optics EXPRESS

Consequently, the outer regions of the Airy-like beams turn farther apart. The Airy-like beams that constitute the Layer beam at the respective distances L_{PL} are illustrated in Figs. 9(d), 9(e), and 9(f). It is evident that the beams turn farther and farther apart from the optical axis as the distance L_{PL} decreases. Due to this, as the distance L_{PL} shortens even more the contrast of the lines decreases until it is not possible to distinguish the line pattern at the optical axis.

For the distance L_{PL} of 26.0 mm, the beam's wavefront is entirely converging (Fig. 5(e)), with no local extrema or inflection points. The straight outer regions of the Airy-like beam intersect the optical axis, resulting in a rapid loss of power in the paraxial region and preventing the beam from propagating to infinity (Fig. 9(d)). The beam propagates only in the near zone and keeps its pseudo-nondiffracting properties along the whole propagation length.

Simulated longitudinal profiles of finite Layer beams, generated using projection lenses with focal lengths (F_{PL}) of 20 mm and 40 mm, are depicted in Fig. 10. The distance L_{Ph} was fixed for both beams at 6 mm, therefore, both beams originate from the same angular phase delay in the spectral domain. As a result, the beams exhibit similar characteristics with finite propagation distances but differ in spatial scaling. The spatial scaling of the Fourier transformation is influenced by the focal length of the projection lens [35], resulting in larger spatial dimensions for beams produced with longer focal lengths. Transversal line profiles were taken at the distance of 0.8 m and 2.5 m, so the generated transversal pattern remained as similar as possible for both beams. A shorter focal length of the projection lens produces a smaller overall beam with finer features.

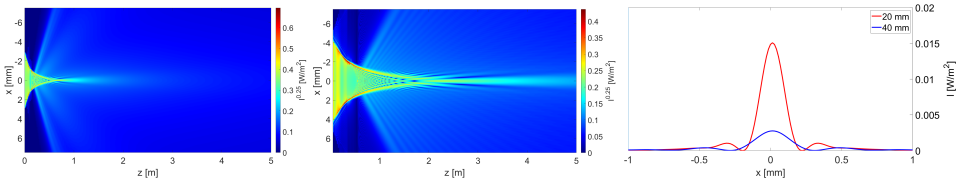

(a) (b) (c)

Fig. 10. Simulated longitudinal profile of finite one-dimensional Layer beams generated using focal length of the projection lens equal to (a) 20 mm, (b) 40 mm for the L_{Ph} of 6 mm. (c) Transversal intensity profile at the distance of 0.8 m from the generator for the focal length of 20 mm, and at 2.5 m from the generator for the focal length of 40 mm.

When a beam propagates to infinity, the stable diverging part of the beam forms at a greater distance for longer focal lengths of the projection lens. As a result, the pattern formed in the diverging region exhibits smaller features. This phenomenon is particularly significant for long-distance alignment, where propagation distances can extend to tens or hundreds of meters. This effect is illustrated in Fig. 11, where the projection lens with a focal length of 40 mm

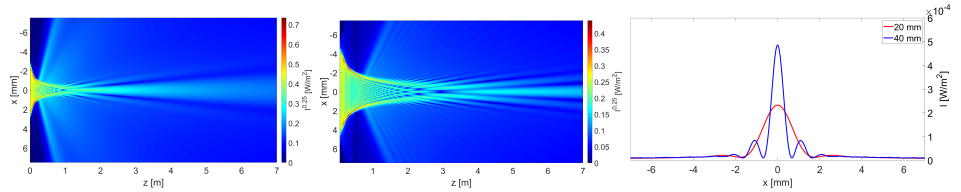

(a) (b) (c)

Fig. 11. Simulated longitudinal profile of infinitely propagating one-dimensional Layer beams generated using focal length of the projection lens equal to (a) 20 mm, (b) 40 mm for the L_{Ph} of 5.6 mm. (c) Transversal line profile at the distance of 7 m from the generator.

Optics EXPRESS

produces a beam with finer features at a distance of 7 m, compared to a focal length of 20 mm. The distance L_{Ph} for both beams was equal to 5.6 mm.

Transversal intensity profiles of a simulated two-dimensional Layer beam at the distance of 1, 1.5, 2, and 2.5 m from the generator are shown in Fig. 12. An additional phase lens with the same parameters was added, along with a projection lens with a focal length of 50 mm, rotated 90 degrees around the optical axis (Fig. 3) with the distance L_{PL1} = 28.6 mm, and the distance L_{PL2} = 55.9 mm. This leads to the creation of a pattern that is composed of two orthogonal Layer beams. At 1.5 m (Fig. 12(a)), noticeable field distortion occurs due to the beam passing through the projection lens, manifesting as curved lines in the pattern. However, this effect diminishes as the beam propagates further.

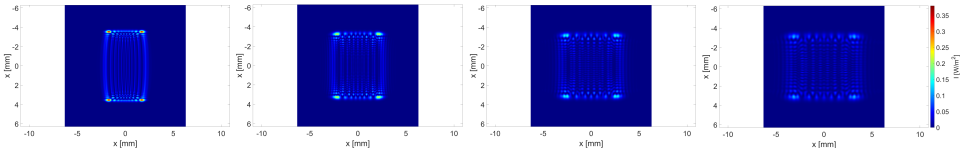

(a) (b) (c) (d)

Fig. 12. Transversal intensity profiles of a simulated two-dimensional Layer beam at: (a) 1 m, (b) 1.5 m, (c) 2 m and (d) 2.5 m.

The generating wavefront of the two-dimensional beam, along with simulated and modeled line profiles according to Eq. (1), are depicted in Fig. 13. The coefficient values are K_1 = -1.32e-6 and K_2 = 2.20e-7 for the x-axis, and K_1 = -3.43e-7 and K_2 = 5.59e-9 for the y-axis. The modeled wavefront along the x-axis does not perfectly match the simulated one due to field distortion caused by the additional projection lens.

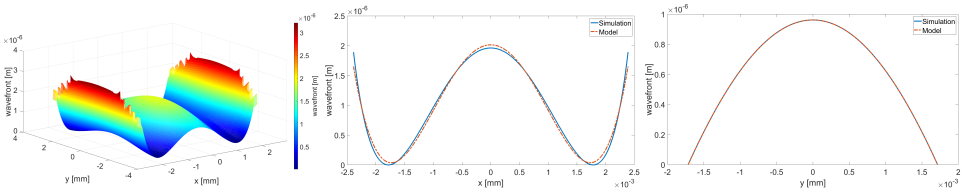

(a) (b) (c)

Fig. 13. (a) Simulated generating wavefront for the two-dimensional Layer beam. (b) Line profile of the generating wavefront along the x-axis, and (c) line profile along the y-axis, with modeled wavefronts according to Eq. (1).

3.2. Measurements

Several Layer beams were generated in the laboratory using the generator with the same parameters as the ones used for the simulations. The phase lens with a focal length of 5.79 mm was used together with the projection lens with a focal length equal to 20 mm. The size of the CMOS sensor was 14.57 mm x 12.6 mm and the wavelength of the Gaussian beam was 532 nm. The wavefront was measured using a Shack-Hartman sensor and reconstructed using an in-house developed software [38]. The sensor was moved as close as possible to the generator, hence the measurement of the generating wavefront was done almost directly behind the projection lens. So-called zonal reconstruction was used which allows for reconstruction of the wavefront in the entire microlens array [38,39].

Transversal intensity profiles of the one-dimensional Layer beam propagating over a limited distance are shown in Fig. 14. The distance L_{PL} was equal to 26.15 mm. Initially, a fine structure

Optics EXPRESS

of lines is observed at a distance of 0.07 m (Fig. 14(a)). As the beam continues to propagate, the number of lines decreases (Figs. 14(b) and 14(c)) until a clear structure is not visible on the camera in 1.3 m (Fig. 14(d)), while only a low-intensity residual can be seen. The measured generating wavefront for the aforementioned beam can be seen in Fig. 15(a) along with the line profile together with the modeled wavefront according to Eq. (1) in Fig. 15(b). The coefficient values K_1 and K_2 are equal to 0.73e-6 and 1.89e-7 respectively. The finite beam exhibits a purely converging shape along this axis.

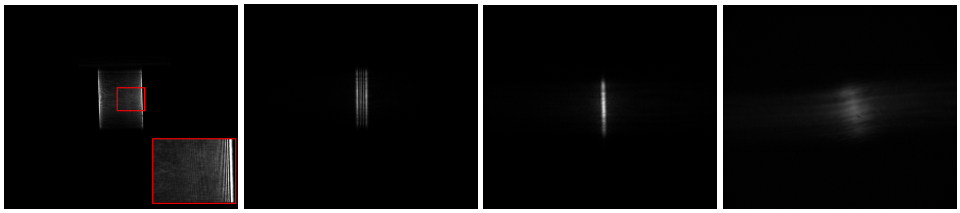

(a) (b) (c) (d)

Fig. 14. Transversal intensity profiles with an enhanced contrast of a one-dimensional Layer beam propagating over a limited distance of: (a) 0.07 m, (b) 0.35 m, (c) 0.70 m and (d) 1.3 m. The size of the image is 14.57 mm x 12.6 mm.

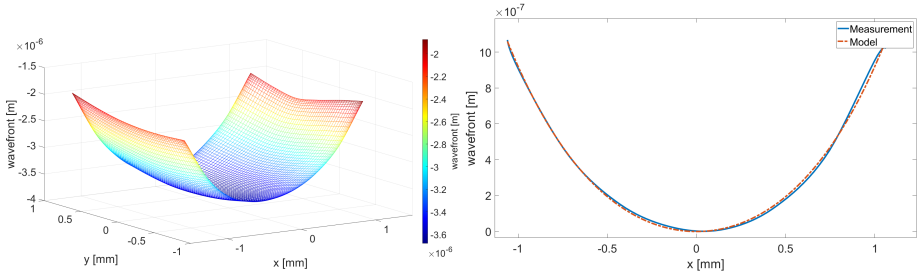

(a) (b)

Fig. 15. (a) Generating wavefront measured using the Shack-Hartmann sensor for the finite Layer beam. (b) Line-profile of the generating wavefront with modeled wavefront according to Eq. (1).

The one-dimensional Layer beam propagating to infinity is depicted in Fig. 16. The distance L_{PL} was equal to 25.25 mm. The number of lines changes as the beam travels in the near zone (Figs. 16(a) and 16(b)). In the diverging zone, the pattern stabilizes, as can be seen for the distances of 4.1 and 5.3 m (Figs. 16(c) and 16(d)). The measured generating wavefront for the aforementioned beam can be seen in Fig. 17(a) and the line profile together with the modeled wavefront according to Eq. (1) in Fig. 17(b). The coefficient values K_1 and K_2 are equal to -0.63e-6 and 1.93e-7 respectively. The local minima in the line profile along the x-axis are evident, the beam propagates to infinity.

The value of K_1 for both one-dimensional beams is slightly outside the expected range obtained from simulations (Fig. 4). This discrepancy may be due to the physical difficulty of measuring the wavefront directly behind the projection lens, as there was a gap of several tens of millimeters between the projection lens surface and the Shack-Hartmann sensor. Alternatively, it could be due to spatial or wavefront differences between the Gaussian beam used in the simulations and the one in the measurements.

A two-dimensional Layer beam is depicted in Fig. 18. Similarly to the simulation, an additional phase lens with the same parameters was added, along with an extra projection lens with a focal

Optics EXPRESS

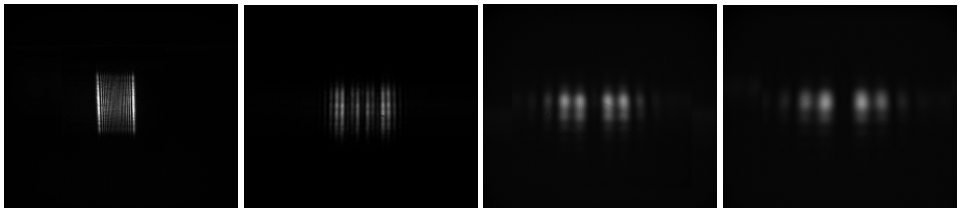

(a) (b) (c) (d)

Fig. 16. Transversal intensity profiles with an enhanced contrast of a one-dimensional infinitely propagating Layer beam at: (a) 0.3 m, (b) 1.25 m, (c) 4.1 m, and (d) 5.3 m. The size of the image is 14.57 mm x 12.6 mm.

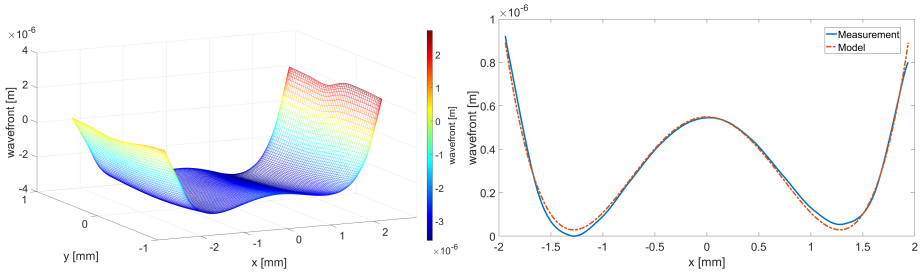

(a) (b)

Fig. 17. (a) Generating wavefront measured using the Shack-Hartmann sensor for the infinitely propagating Layer beam. (b) Line-profile of the generating wavefront with modeled wavefront according to Eq. (1).

length of 50 mm rotated 90 degrees around the optical axis (Fig. 3) with the distance L_{PL1} = 29 mm, and the distance L_{PL2} = 55.6 mm. At the distance of 0.15 m (Fig. 18(a)), noticeable field distortion occurs because the beam passes through an additional projection lens, which manifests itself as curved lines in the pattern. However, this effect diminishes as the beam travels further.

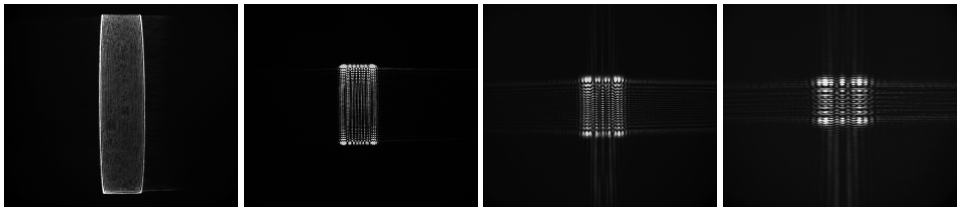

(a) (b) (c) (d)

Fig. 18. Transversal intensity profiles with an enhanced contrast of a two-dimensional Layer beam at: (a) 0.15 m, (b) 0.85 m, (c) 1.10 m and (d) 1.80 m. The size of the image is 14.57 mm x 12.6 mm.

The measured generating wavefront of the two-dimensional Layer beams is depicted in Fig. 19(a). The line profiles together with the modeled wavefront according to Eq. (1) with coefficients values K_1 = -1.14e-6 and K_2 = 2.23e-7 for the line-profile along the x-axis and K_1 = -5.34e-7 and K_2 = 8.43e-9 for the line-profile along the y-axis can be seen in Figs. 19(b) and 19(c) respectively. The distinctive sombrero shape of the line profile is observed along the x-axis while only the diverging part of the wavefront is visible along the y-axis.

Optics EXPRESS

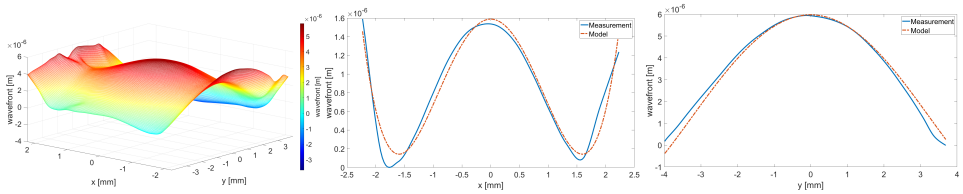

(a) (b) (c)

Fig. 19. (a) Generating wavefront measured using the Shack-Hartmann sensor for the two-dimensional Layer beam. (b) Line-profile of the generating wavefront along the x-axis. (c) Line-profile of the generating wavefront along the y-axis with modeled wavefronts according to Eq. (1).

Generating the two-dimensional beams, using only a single optical element that can introduce a phase shift similar to the generating wavefront, or using a spatial light modulator would mitigate this distortion. Nevertheless, there will be a trade-off in the cost of the setup and the tunability of the beam parameters compared to the generation using cylindrical lenses. An alternative approach involves combining two orthogonal Layer beams using a beam splitter, however, this configuration imposes requirements on the precise alignment of the beams.

4. Discussion

In this study, pseudo-nondiffracting one-dimensional and two-dimensional Layer beams were successfully simulated and generated using various combinations of cylindrical lenses. The simulations confirmed that, depending on the generator parameters, a Layer beam can be tuned to propagate over finite or infinite distances based on the shape of the generating wavefront. The relationship between the generating wavefront shape and the beam's propagation characteristics was analyzed, revealing a connection to the propagation behavior of the two Airy-like beams that form the Layer beam.

Most of the simulations focused on the one-dimensional beam. For beams with finite propagation distances, the number of lines gradually decreased as the beam propagated, exhibiting pseudo-nondiffracting properties, such as regeneration behind obstacles throughout the entire propagation length. For beams propagating over infinite distances, the pattern stabilized after leaving the near zone and entering a so-called diverging zone. In this case, the infinitely propagating beam maintained a consistent transversal intensity distribution pattern that diverged further along the propagation path, losing its pseudo-nondiffracting properties. By adjusting the focal length of the projection lens, the beam's spatial dimensions can be tailored to a given distance.

The two-dimensional Layer beam, while demonstrating similar characteristics, showed initial shape distortions due to the additional projection lens. However, these distortions became negligible as the beam propagated further, indicating that initial aberrations introduced by optical elements can be mitigated with sufficient propagation distance. The ability to generate such beams with cylindrical lenses underscores the versatility and effectiveness of this approach while maintaining a low-cost, low-complexity setup.

The propagation characteristics of the Layer beams were confirmed through measurements. The generating wavefronts, measured using a Shack-Hartmann sensor, closely matched the simulated wavefronts. Discrepancies between measurements and simulations may have arisen due to spatial constraints that prevented direct wavefront measurement immediately behind the projection lens or differences between the Gaussian beams used in the simulations and those in the experiments.

Optics EXPRESS

Overall, this work demonstrates the feasibility of generating Layer beams using cylindrical lenses, providing a solid foundation for further exploration of these beams in various applications. Future research will focus on developing a system that utilizes Layer beams specifically for the alignment of accelerator components.

Funding. Technická Univerzita v Liberci (SGS-2024-3423); CERN.

Acknowledgments. The authors acknowledge the financial support provided by the Knowledge Transfer group at CERN through the KT Fund. Portions of this work were presented at the IPAC2024 conference, Optimization of Symmetrical Optical Caustic Beams for Long-Distance Alignment, and at the conference EUSPEN2024, Optimization of Symmetrical Layers of Optical Caustic Beams Generated Using Cylindrical Lenses. This work was partly supported by the Student Grant Scheme at the Technical University of Liberec through project SGS-2024-3423.

Disclosures. The authors declare no conflicts of interest.

Data availability. Data underlying the results presented in this paper are not publicly available at this time but may be obtained from the authors upon reasonable request.

References

1. Y. A. Kravtsov and Y. I. Orlov, *Caustics, Catastrophes and Wave Fields*, vol. 15 (Springer Science & Business Media, 2012).
2. J. F. Nye, *Natural Focusing and Fine Structure of Light: Caustics and Wave Dislocations* (CRC Press, 1999).
3. P. Vaveliuk, A. Lencina, J. A. Rodrigo, *et al.*, "Caustics, catastrophes, and symmetries in curved beams," Phys. Rev. A **92**(3), 033850 (2015).
4. G. A. Siviloglou and D. N. Christodoulides, "Accelerating finite energy airy beams," Opt. Lett. **32**(8), 979–981 (2007).
5. G. Siviloglou, J. Broky, A. Dogariu, *et al.*, "Observation of accelerating airy beams," Phys. Rev. Lett. **99**(21), 213901 (2007).
6. T. Vettenburg, H. I. Dalgarno, J. Nylk, *et al.*, "Light-sheet microscopy using an airy beam," Nat. Methods **11**(5), 541–544 (2014).
7. J. Baumgartl, M. Mazilu, and K. Dholakia, "Optically mediated particle clearing using airy wavepackets," Nat. Photonics **2**(11), 675–678 (2008).
8. P. Polynkin, M. Kolesik, J. V. Moloney, *et al.*, "Curved plasma channel generation using ultraintense airy beams," Science **324**(5924), 229–232 (2009).
9. N. K. Efremidis, Z. Chen, M. Segev, *et al.*, "Airy beams and accelerating waves: an overview of recent advances," Optica **6**(5), 686–701 (2019).
10. P. Vaveliuk, A. Lencina, J. A. Rodrigo, *et al.*, "Symmetric airy beams," Opt. Lett. **39**(8), 2370–2373 (2014).
11. P. Vaveliuk, A. Lencina, J. A. Rodrigo, *et al.*, "Intensity-symmetric airy beams," J. Opt. Soc. Am. A **32**(3), 443–446 (2015).
12. Y. Wu, J. Zhao, Z. Lin, *et al.*, "Symmetric pearcey gaussian beams," Opt. Lett. **46**(10), 2461–2464 (2021).
13. Q. Wei, J. Jiang, Z. Mo, *et al.*, "Symmetric swallowtail beams in the rectangle frame," Ann. Phys. **535**(3), 2200466 (2023).
14. J. Wang, J. Bu, M. Wang, *et al.*, "Generation of high quality airy beams with blazed micro-optical cubic phase plates," Appl. Opt. **50**(36), 6627–6631 (2011).
15. A. Benstiti, K. Ferria, and A. Bencheikh, "Generation of a variety of airy beams using a dynamic diffractive optical phase element," J. Opt. Soc. Am. B **37**(11), A45–A53 (2020).
16. B. Yalizay, B. Soylu, and S. Akturk, "Optical element for generation of accelerating airy beams," J. Opt. Soc. Am. A **27**(10), 2344–2346 (2010).
17. L. Begel and T. Galstian, "Dynamic generation of non-diffracting beams by using an electrically variable liquid crystal lens," Opt. Commun. **441**, 127–131 (2019).
18. J. Ma, Y. Li, Q. Yu, *et al.*, "Generation of high-quality tunable airy beams with an adaptive deformable mirror," Opt. Lett. **43**(15), 3634–3637 (2018).
19. B. Wu, B. Xu, X. Wang, *et al.*, "Generation of a polarization insensitive airy beam using an all-dielectric metasurface," Opt. Mater. Express **11**(3), 842–847 (2021).
20. B. Yu, J. Wen, L. Chen, *et al.*, "Polarization-independent highly efficient generation of airy optical beams with dielectric metasurfaces," Photonics Res. **8**(7), 1148–1154 (2020).
21. Z. Cai, Y. Liu, C. Zhang, *et al.*, "Continuous cubic phase microplates for generating high-quality airy beams with strong deflection," Opt. Lett. **42**(13), 2483–2486 (2017).
22. B.-Y. Wei, P. Chen, W. Hu, *et al.*, "Polarization-controllable airy beams generated via a photoaligned director-variant liquid crystal mask," Sci. Rep. **5**(1), 17484 (2015).
23. J. Zhou, Y. Liu, Y. Ke, *et al.*, "Generation of airy vortex and airy vector beams based on the modulation of dynamic and geometric phases," Opt. Lett. **40**(13), 3193–3196 (2015).
24. Z. Cao, C. Zhai, J. Li, *et al.*, "Light sheet based on one-dimensional airy beam generated by single cylindrical lens," Opt. Commun. **393**, 11–16 (2017).

Optics EXPRESS

25. D. Papazoglou, S. Suntsov, D. Abdollahpour, *et al.*, "Tunable intense airy beams and tailored femtosecond laser filaments," Phys. Rev. A **81**(6), 061807 (2010).
26. D. Abdollahpour, M. Lotfollahi, M. Yeganeh, *et al.*, "Generation and characterization of adjustable pure third-order spatial phase by tuning optical aberrations," J. Opt. **21**(8), 085602 (2019).
27. Z. Yang, M. Prokopas, J. Nylk, *et al.*, "A compact airy beam light sheet microscope with a tilted cylindrical lens," Biomed. Opt. Express **5**(10), 3434–3442 (2014).
28. W. Niewiem, K. Polak, M. Dusek, *et al.*, "Variation of structured laser beam pattern and optimization for an alignment reference line creation," Opt. Express **31**(26), 43307–43322 (2023).
29. M. Dusek, E. Roikova, D. Mergelkuhl, *et al.*, "Analysis of centroiding algorithms for non-diffracting structured and hollow structured laser beams," Appl. Opt. **63**(1), 263–274 (2024).
30. M. Dusek, J.-C. Gayde, and M. Sulc, "Wavefront reconstruction of a non-diffracting structured laser beam," Opt. Express **31**(25), 42099–42110 (2023).
31. K. Polak, M. Sulc, and J.-C. Gayde, "Structured laser beam in non-homogeneous environment," in *15th International Workshop on Accelerator Alignment* (2022).
32. K. Polak, J. Gayde, S. M. Sulc, *et al.*, "3D Polarisation of a Structured Laser Beam and Prospects for its Application to Charged Particle Acceleration," in *14th International Particle Accelerator Conference* (2023), pp. 1444–1445.
33. H. M. Durand, S. Bartolome-Jimenez, T. Dijoud, *et al.*, "HL-LHC Alignment Requirements and Associated Solutions," in *Proc. IPAC* (JACoW Publishing, 2017), pp. 1893–1896.
34. J. Gayde and M. Sulc, "An optical system for producing a structured beam," EP3564734 (2019).
35. J. W. Goodman, *Introduction to Fourier Optics* (Roberts and Company Publishers, 2005).
36. J. Durmin, "Exact solutions for nondiffracting beams," J. Opt. Soc. Am. A **4**(4), 651–654 (1987).
37. M. Born and E. Wolf, *Principles of Optics: Electromagnetic Theory of Propagation, Interference and Diffraction of Light* (Elsevier, 2013).
38. M. Dusek, "Advanced calibration and characterization of a Shack-Hartmann sensor," Master's thesis, Technical University of Liberec (2021).
39. W. H. Southwell, "Wave-front estimation from wave-front slope measurements," J. Opt. Soc. Am. **70**(8), 998–1006 (1980).